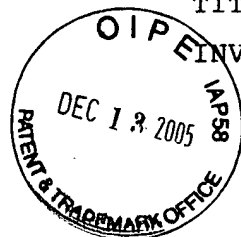


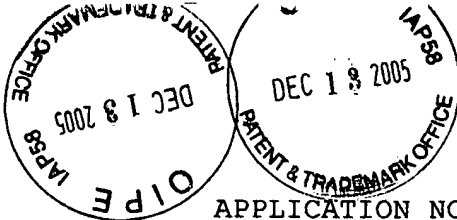
APPLICATION NO. 09/826,118

TITLE OF INVENTION: Wavelet Multi-Resolution Waveforms



INVENTOR: Urbain A. von der Embse

Clean version of how the SPECIFICATION  
Will read.



APPLICATION NO.

09/826,118

TITLE OF INVENTION: Wavelet Multi-Resolution Waveforms

INVENTOR: Urbain A. von der Embse

5

## BACKGROUND OF THE INVENTION

### I. Field of the Invention

10

The present invention relates to CDMA (Code Division Multiple Access) cellular telephone and wireless data communications with data rates up to multiple T1 (1.544 Mbps) and higher (>100 Mbps), and to optical CDMA. Applications are mobile, point-to-point and satellite communication networks. More specifically the present invention relates to a new and novel means for a new approach to the design of waveforms and filters using mathematical formulations which generalize the Wavelet concept to communications and radar.

20

### II. Description of the Related Art

25

Multi-resolution waveforms used for signaling and/or filters and which are addressed in this invention are defined to be waveforms of finite extent in time and frequency, with scale and shift properties of multi-resolution over the time-frequency (t-f) space. These waveforms can also be referred to as multi-scale waveforms, and include multi-rate filtering and the Wavelet as special cases. The emphasis will be on digital design and applications with the understanding that these multi-resolution waveforms are equally applicable to analog design and applications.

35

Background art consists of the collection of waveform and filtering design techniques which can be grouped into six broad categories. These categories are: C1) least squares (LS) design algorithms for filters and waveforms that design to specifications on their frequency response, C2) analytic filters and waveforms which are specified by a few free design parameters that can be sub-categorized into current applications and primarily theoretical studies, C3) combinations of C1 and C2 for greater flexibility in meeting communications and radar performance goals, C4) special design techniques to control the noise levels from intersymbol interference (ISI) and adjacent channel interference (ACI) in the presence of timing offsets for multiple channel applications, C5) Wavelet filter design using scaling functions (iterated filter banks) as the set of design coordinates or basis functions, C6) filter and waveform design techniques for non-linear channels and in particular for operation in the non-linear and saturation regions of a high power amplifier (HPA) such as a traveling wave tube (TWT) or a solid state amplifier, and C7) LS dynamic filters derived from discrete filtering and tracking algorithms that include adaptive equalization for communications, adaptive antenna filters, Wiener filters, Kalman filters, and stochastic optimization filters.

Category C1 common examples of LS digital filter design are the eigenvalue algorithm in "A New Approach to Least-Squares FIR Filter Design and Applications Including Nyquist Filters" and the Remez-Exchange algorithm in "A Computer Program for Designing Optimum FIR Linear Phase Filters". The eigenvalue algorithm is a direct LS minimization and the Remez-Exchange can be reformulated as an equivalent LS gradient problem through proper choice of the cost function. Both LS algorithms use the FIR (finite impulse response) digital samples as the set of design coordinates. LS design metrics are the error residuals in meeting their passband and stopband ideal performance as shown in FIG. 3. Category C2

common examples of analytical waveforms and filters for system applications are the analog Chebyshev, Elliptic, Butterworth, and the digital raised-cosine, and square-root raised-cosine. For theoretical studies, common examples are polyphase multirate  
5 filters, quadrature mirror filters (QMF), and perfect reconstruction filters. Although these theoretical studies have yet to yield realizable useful filters for system applications, their importance for this invention lies in their identification and application of ideal performance metrics for filter  
10 designs. Category C3 common digital example is to start with the derivation of a Remez-Exchange finite impulse response (FIR) filter and then up-sample and filter with another bandwidth limiting filter. This results in an FIR over the desired frequency band that is larger than available with the Remez-  
15 Exchange algorithm and with sidelobes that now drop off with frequency compared to the flat sidelobes of the original Remez-Exchange FIR. A category C4 common example is to select the free parameters of the category C3 filter in order to minimize the signal to noise power ratio of the data symbol (SNR) losses from  
20 the ISI, ACI, and the non-ideal demodulation. A second common example is start with a truncated pulse whose length is short enough compared to the symbol repetition interval, to accommodate the timing offsets without significant impact on the ISI and ACI SNR losses. This shortened pulse can then be shaped in the  
25 frequency domain.

Category C5 Wavelet filter design techniques discussed in the next section will serve as a useful reference in the disclosure of this invention. Category C6 common example is the  
30 Gaussian minimum shift keying (GMSK) waveform. This is a constant amplitude phase encoded Gaussian waveform which has no sidelobe re-growth through a non-linear or saturating HPA. Category C7 common examples are the adaptive equalization filter for communication channels, the adaptive antenna filter,

and the Kalman filter for applications including target tracking and prediction as well as for equalization and adaptive antennas.

Minimizing excess bandwidth in the waveform and filter design is a key goal in the application of the C1,...,C6 design techniques for communications and radar. Excess bandwidth is identified as the symbol  $\alpha$  in the bandwidth-time product  $BT_s = 1 + \alpha$  where the two-sided available frequency band is  $B$  and the symbol repetition interval is  $T_s$ . Current performance capability is represented by the use of the square-root raised cosine (sq-rt rc) waveform with  $\alpha = 0.22$  to  $0.4$  as shown in FIG. 6. The goal is to design a waveform with  $\alpha = 0$  within the performance constraints of ISI, ACI, passband, sideband, and passband ripple. This goal of eliminating the excess bandwidth corresponds to the symbol rate equal to the available frequency band  $1/T_s = B/(1 + \alpha) = B$  for  $\alpha = 0$ . This symbol rate  $1/T_s = B$  is well known to be the maximum possible rate for which orthogonality between symbols is maintained. A fundamental performance characteristic of our new waveform designs is the ability to eliminate excess bandwidth for many applications.

Scope of invention will include all of the waveform and filter categories with the exception of category C4 special design techniques and category C7 LS dynamic filters. Emphasis will be on the category C5 Wavelets to establish the background art since Wavelets are multi-resolution waveforms that can eliminate the excess bandwidth and have known design algorithms for FIR waveforms and filters. However, they do not have a design mechanism that allows direct control of the ISI, ACI, passband, sideband, and passband ripple. Category C2 theoretical studies also eliminate the excess bandwidth. However, they are not multi-resolution waveforms and do not have realizable FIR design algorithms. So the emphasis in background art will be on Wavelets whose relevant properties we briefly review.

Wavelet background art relevant to this invention consists of the discrete Waveform equations and basic properties, application of Wavelets to cover a discrete digital time-frequency (t-f) signal space, and the design of Wavelets using the iterated filter construction. Wavelets are waveforms of finite extent in time (t) and frequency (f) over the t-f space, with multi-resolution, scaling, and translation properties. Wavelets over the analog and digital t-f spaces respectively are defined by equations (1) and (2) as per Daubechies's "Ten Lectures on Wavelets", Philadelphia:SIAM, 1992

#### Continuous wavelet

$$\psi_{a,b}(t) = |a|^{-1/2} \psi\left(\frac{t-b}{a}\right) \quad (1)$$

#### Discrete wavelet

$$\psi_{a,b}(n) = |a|^{-1/2} \psi\left(\frac{n-b}{a}\right) \quad (2)$$

where the two index parameters "a,b" are the Wavelet dilation and translation respectively or equivalently are the scale and shift. The  $\psi$  is the "mother" wavelet and is a real and symmetric localized function in the t-f space used to generate the doubly indexed Wavelet  $\psi_{ab}$ . The scale factor " $|a|^{-1/2}$ " has been chosen to keep the norm of the Wavelet invariant under the parameter change "a,b". Norm is the square root of the energy of the Wavelet response. The Wavelets  $\psi_{a,b}$  and  $\psi$  are localized functions in the t-f space which means that both their time and frequency lengths are bounded. The discrete Wavelet has the time "t" replaced by the equivalent digital sample number "n" assuming the waveform is uniformly sampled at "T" second intervals.

Wavelets in digital t-f space have an orthogonal basis that is obtained by restricting the choice of the parameters "a,b" to the values  $a=2^{-p}$  ,  $b=qM2^p$  where 'p,q' are the new scale and translation parameters and "M" is the spacing or repetition interval  $T_s=MT$  of the Wavelets (which from a communications viewpoint are symbols) at the same scale "p". Wavelets at "p,q" are related to the mother Wavelet by the equation

$$\begin{aligned}\psi_{p,q}(n) &= 2^{-p/2} \psi(n - qM2^p) \\ &= 2^{-p/2} \psi(2^{-p}n - qM)\end{aligned}\tag{3}$$

where the mother Wavelet is a real and even function of the sample coordinates. The orthonormality property means that these Wavelets satisfy the orthogonality equation with a correlation value equal to "1".

$$\begin{aligned}\sum_n \psi_{p,q} \psi_{k,m} &= 1 \text{ iff both } p = k \text{ and } q = m \\ &= 0 \text{ otherwise}\end{aligned}\tag{4}$$

Wavelet representation of a digital t-f space starts with selecting an N sample time window of a uniform stream of digital samples at the rate of 1/T Hz (1/second) equivalent to a "T" second sampling interval. The N point or sample t-f space in FIG. 1 illustrates a Wavelet representation or "tiling" with Wavelets that are designed analytically or by an iterated filter construction.

The t-f space in FIG. 1 is partitioned or covered or tiled by a set of Wavelet subspaces  $\{W_p, p=0,1,\dots,m-1\}$  where  $N=2^m$ . Each Wavelet subspace  $W_p$  at scale "p" consists of the set of Wavelet time translations  $\{q = 0,1,\dots, N/2^{p+1}-1\}$  over this subspace. These Wavelet subspaces are mutually orthogonal and the Wavelets within

each subspace are mutually orthogonal with respect to the time translates. This N-point t-f space extends over the time interval from 0 to (N-1)T <sup>2</sup> where T is the digital sampling interval, and over the frequency interval from 0 to (N-1) <sup>3</sup> in units of the normalized frequency fNT <sup>4</sup>.

The iterated filter bank in FIG. 2 is used to generate the Wavelets which cover the t-f space in FIG. 1. Each filter stage <sup>5</sup> consists of a high pass filter (HPF) and a low pass filter (LPF). Output <sup>6</sup> of the LPF is subsampled by 2 which is equivalent to decimation by 2. This t-f space space is an N-dimensional complex vector metric space  $V$  <sup>7</sup>. At stage m in the iterated filter bank, the remaining t-f space  $V_{m-1}$  <sup>8</sup> is partitioned into  $V_{m+1}$  <sup>9</sup> and the Wavelet subspace  $W_{m+1}$  <sup>10</sup>.

15

Scaling functions and Wavelets at each stage of this filter bank satisfy the following equations

$$\begin{aligned}\varphi(n) &= 2^{-1/2} \sum_q h_q \varphi(2n-q) \quad \forall q \\ \psi(n) &= 2^{-1/2} \sum_q g_q \varphi(n-q) \quad \forall q\end{aligned}\tag{5}$$

20

where  $\varphi$  is the scaling function,  $\psi$  is the Wavelet,  $HPF_p$  coefficients are  $\{h_q, \forall q\}$ ,  $LPF_p$  coefficients are  $\{g_q, \forall q\}$ , and the equations apply to the stages 0,1,...,m-1. Identifying the scale parameter and using the previous Wavelet formulations enable these equations to be rewritten for stages  $p=0,1,...,m-1$  as

25

$$\begin{aligned}\varphi_p &= \sum_q h_q \varphi_{p-1,q} \quad \forall p \\ \psi_p &= \sum_q g_q \varphi_{p-1,q} \quad \forall p\end{aligned}\tag{6}$$



For our application the  $HPF_p$  and  $LPF_p$  are quadrature mirror filters (QMF) with perfect reconstruction. This means they cover the subspace  $V_p$  with flat responses over the subband frequency including the edges of the frequency subband, and the  $HPF_p$  coefficients are the frequency translated coefficients for the  $LPF_p$ :  $\{g_q = (-1)^q h_q, \forall q\}$ .

Wavelet design using iterated filter bank starts with the selection of the scaling functions. Starting with a primitive scaling function such as the one proposed by Daubechies' one can use the iterated filter construction given by equations (5) and (6) to derive successive approximations to a desired scaling function which has properties that have been designed into it by the selection of the filter coefficients  $\{g_q, \forall q\}$  at each level of iteration. The Wavelets can be derived from these scaling functions using the iterated filter construction or scaling equations (5) and (6).

Another use of the iterated filter construction is to design the scaling functions as Wavelets thereupon ending up with a larger set of Wavelets for multi-resolution analysis and synthesis as illustrated by Coifman's Wavelets in "Wavelet analysis and signal processing".

## SUMMARY OF THE INVENTION

This invention is a new and novel design of Wavelet multi-resolution waveforms and filters in the frequency domain with a property which provides a single waveform design for all of the waveforms at multiple resolutions and scales. Wavelets are designed to meet the specific application requirements, are complex, are defined by frequency harmonics, include a frequency translation parameter in addition to the scale and translation parameters in current Wavelets, and have the property that the set of design coefficients in the frequency domain remain invariant for all possible multi-resolution scales, and time-frequency translations. Frequency design harmonics and the frequency translation capability enable the waveforms at multiple resolution scales to be derived from the single waveform design by scaling the dilation, translation, and frequency translation parameters using the set of frequency design harmonics. Wavelet waveform design is illustrated by Matlab 5.0 code to design a linear filter waveform using an iterative least-squares eigenvalue approach to minimize the non-linear least-squares cost function, and to scale this waveform design for multi-resolution application specified by the dilation, time translation, and frequency translation parameters. Additional results are given for a constant amplitude minimum-shift-keying bandwidth-efficient modulation waveform and for a synthetic aperture radar waveform.

This invention is a new approach to the design of multi-resolution waveforms that improves their performance for engineering and scientific applications, and in particular for applications to communications and radar. Current practice is to 1) design traditional multi-resolution waveforms in the time domain using metrics which specify frequency performance and without consideration of Wavelet properties or to 2) design Wavelet multi-resolution waveforms using the time-domain iterated

multi-resolution filtering approach with a set of scaling functions used to perform the filtering and without direct considerations of the frequency performance. These two separate design approaches yield fundamentally different waveforms. Our new invention provides a means to combine these two approaches to generate a new multi-resolution waveform with the best properties of the traditional multi-resolution waveforms and the Wavelet multi-resolution waveform.

## BRIEF DESCRIPTION OF THE DRAWINGS AND THE PERFORMANCE DATA

The above-mentioned and other features, objects, design algorithms, and performance advantages of the present invention will become more apparent from the detailed description set forth below when taken in conjunction with the drawings and performance data wherein like reference characters and numerals denote like elements, and in which:

FIG. 1 is a Wavelet N-point t-f space extending over the time interval  $(0, (N-1)T]$  and the frequency interval  $(0, (N-1)/NT]$ , which is tiled or covered by a set of orthonormal Wavelets at the scales  $p=0,1,\dots,m-1$ .

FIG. 2 is a Wavelet iterated filter bank used to generate the set of Wavelets which tile or cover the t-f space in FIG. 1.

FIG. 3 is the power spectral density (PSD) template for the the stopband and passband used to construct the LS error metrics,

FIG. 4 is the flow diagram of the LS metrics and cost functions and the final cost function used to find the optimal LS solution for the Wavelet waveform.

5        FIG. 5 is the Matlab 5.0 code for the LS algorithm used to design the Wavelet waveform in FIG. 6.

10        FIG. 6 plots the dc PSD in dB units for the frequency response of the mother Wavelet at dc and the square-root raised-cosine (sq-rt r-c) waveforms with excess bandwidth parameter  $\alpha = 0.22, 0.40$  vs. the normalized frequency in units of symbol rate  $1/T_s$ .

15        FIG. 7 plots the dc PSD in dB units for the frequency response of the mother Wavelet at dc and an optimized Gaussian minimum shift keying (GMSK) waveform vs. the normalized frequency  $fT_s$ .

20        FIG. 8 plots the amplitude of the dc radar ambiguity function vs. the normalized frequency  $fT_p$  and normalized time  $tT_c$  where the pulse time  $T_p$  and chip time  $T_c$  are both equal to the communications symbol interval  $T_s$  for this example, for the new waveform and an unweighted chirp waveform.

25

30

35

## DISCLOSURE OF THE INVENTION

Wavelet multi-resolution waveforms incorporate a frequency translation, are complex, are designed in frequency harmonic coordinates, a single mother Wavelet design is used for all scales, and in the t-f space are realized as FIR filters and waveforms.

These Wavelet waveforms in this invention disclosure are generalizations of Wavelets in t-f space which enable them to be useful for communications and radar applications. This generalization is accomplished by 1) the introduction of a frequency translation, by 2) changing the orthonormality condition in equation (4) to apply to waveforms within the same space {q} and over the scales {p} with the inclusion of the frequency translation, and 3) by their characterization and design in the Fourier domain. With frequency translation the analytical formulation of these new waveforms as a function of the baseband or mother waveform centered at dc( dc refers to the origin  $f=0$  of the frequency space) becomes

$$\psi_{p,q,r}(n) = 2^{-p/2} \psi(2^{-p}n - qM) e^{i2\pi f_c(p,r)nT} \quad (7)$$

where  $f_c(p,r)$  is the center frequency of the frequency translated dc waveform, at scale "p" and frequency index "r". The purpose of the frequency index "r" is to identify the center frequencies of the waveforms at the scale "p" in the t-f space. The dc or baseband or mother waveform is the generalization of the mother Wavelet for multi-resolution waveforms.

These waveforms satisfy the complex orthonormality equations

$$\sum_n \psi_{p,q,r} \psi_{k,m,v}^* = 1 \text{ iff } p=k \text{ and } q=m \text{ and } r=v$$

$$=0 \text{ otherwise} \quad (8)$$

where "\*" is conjugation, and are generalizations of the  
 5 orthonormality equations for the analytical Wavelets in (4).

These waveforms are generalizations of Wavelets in the  
 frequency domain using a means which makes them useful for  
 communications and radar in the t-f space. The basis vectors for  
 10 this metric space  $V$  consist of a subset of the admissible set  
 of scaled and translated waveforms  $\{\psi_{p,q,r}, \forall p,q,r\}$  derived from the  
 dc waveform  $\psi$  as per equation (7). An admissible waveform is  
 any combination that covers  $V=t-f$  space. We are interested in  
 the Fourier domain representation of the dc waveform  $\psi$  in  $V$ ,  
 15 and in particular in a subset of the discrete Fourier transform  
 (DFT) harmonic coefficients over the Fourier domain which we  
 intend to use as the design coordinates. Starting with the z-  
 transform and continuous Fourier transform, the DFT harmonic  
 coefficients are defined by the following equations

20

DFT Harmonic Coefficients (9)

$$\psi(z) = \sum_n \psi(n) z^{-n} \quad \text{z-transform}$$

$$\psi(\omega) = \sum_n \psi(n) e^{-j\omega n} \quad \text{Fourier transform}$$

$$\psi_k = \sum_n \psi(n) W_N^{-kn} \quad \text{DFT harmonic coefficients for } \forall k$$

where

$$\begin{aligned}\psi(\omega) &= (1/N') \sum_k \Psi_k \sum_n e^{i(2\pi k/N' - \omega)n} \\ &= \sum_k \psi_k \sin((\omega/2 - \pi k/N')N') / N \sin(\omega/2 - \pi k/N') \\ &= \sum_k \psi_k [\text{Harmonic interpolation for "k"}]\end{aligned}$$

$$W_{N'}^{kn} = e^{i2\pi kn/N'}$$

$\{k\}$  = DFT frequency or harmonic coefficients such that  $f_k = k/N'T$   
 where  $f_k$  is the harmonic frequency corresponding to "k"

$N'$  = length of  $\psi(n)$

where  $\Psi(\omega) = |\psi(\omega)|^2$  is the power spectral density of the dc waveform. These equations define the frequency representation of our new waveforms in terms of the available set of harmonic coefficients, which set is considerable larger than required for most applications.

Wavelet waveforms have . orthonormality and no excess bandwidth properties which are asymptotically approached to within design accuracies inherent in communications and radar. To demonstrate these properties we need to identify the structure of the dc waveform in  $V$ . We start with definitions for the parameters and coordinates in the following equation (10). The waveforms derived from the dc waveform will be designed to be orthogonal over both time translates "MT" and frequency translates "1/MT" which respectively correspond to the Wavelet symbol spacing  $T_s = MT$  and the adjacent channel spacing  $1/T_s$ . This means the orthogonal spacing of the waveforms in  $V$  are at the time-frequency increments  $(MT, 1/MT) = (T_s, 1/T_s)$ . In the interests of constructing our orthonormal multi-resolution waveforms to cover  $V$  it will be convenient to assume that  $M, L$  are powers of 2. We need the following definitions for the parameters and coordinates.

- $N'$  = Length of  $\psi$  which is an even function about the center and  
 which spans an odd number of points or samples  
 =  $ML + 1$  where  $M, L$  are assumed to be even functions for  
 convenience of this analysis  
 = Number of points of  $\psi$   
 $M$  = Sampling interval for  $\psi$   
 = Spacing of  $\psi$  for orthogonality  
 $L$  = Length of  $\psi$  in units of the sample interval  $M$   
 = Stretching of  $\psi$  over  $L$  sample intervals  
 $n$  =  $n_0 + n_1 M$   
 = partitioning into an index  $n_0$  over the sample  
 length  $n_0 = 0, 1, \dots, M - 1$  and an index  $n_1 = 0, 1, \dots, L - 1$   
 over the sample intervals  
 $k$  =  $k_0 + k_1 L$   
 = partitioning into an index  $k_0$  over the harmonic  
 frequencies  $k_0 = 0, 1, \dots, L - 1$  corresponding to the  
 stretching and an index  $k_1 = 0, 1, \dots, M$  over the harmonics  
 frequencies corresponding to the admissible frequency  
 slots for  $\psi$

The harmonic design coordinates are selected using the  
 5 following observation. For most applications and in the following  
 development it is assumed that the waveforms are spectrally  
 contained in the frequency interval  $1/MT$  corresponding to the  
 frequency spacing. This suggests the harmonic design coordinates  
 be restricted to the subset of  $L$  harmonics  $\{k_0=0, 1, \dots, L-1\}$   
 10 covering this spacing. These  $L$  harmonics correspond to the  
 stretching of the mother waveform over the  $L$  repetition  
 intervals.

Obviously, for some applications as will be demonstrated  
 15 later, the spectral containment is spread out over several  $1/LT$



frequency increments whereupon one must increase the subset of design harmonics to possibly 2L, 3L or larger.

Pursuing this application using L design harmonics, the DFT equations for the dc waveform in (9) when rewritten in terms of the L harmonic design coordinates  $\{\psi_{k_0}, \forall k_0\}$  become:

DFT equations for dc waveform

$$\begin{aligned} \psi_{k_0} &= \sum_n \psi(n) W_N^{k_0 n} \quad \text{harmonic design coordinates} \\ \psi(n) &= (1/N) \sum_{k_0} \psi_{k_0} W_N^{k_0 n} \quad \text{new waveform defined in terms} \quad (11) \\ &\quad \text{of the L harmonic design coordinates } \{\psi_{k_0}, \forall k_0\} \end{aligned}$$

It will be proven that the use of these L harmonic design coordinates is sufficient under time translates to be a basis for the corresponding subspace of  $V$  which means these waveforms provide a complete set of coordinates to describe this subspace. The proof will use the theorems of Karhunen-Loeve and Mercer and will limit the demonstration to the dc waveform for simplicity and without loss of generality. Consider the expansion of a random complex sequence  $\{z(n), \forall n\}$  in a series of waveform coordinates consisting of time translates of the mother waveform  $\psi$ . The sequence  $\{z(n), \forall n\}$  is a zero-mean stationary random process which is orthonormal over the sample interval "M" and has a frequency spectrum which is flat and extends over the frequency range  $1/LT$  which is centered at baseband corresponding to a zero frequency. This means the  $\{z(n), \forall n\}$  cover the subspace of  $V$  corresponding to the scale of our dc waveform  $\psi$  and its time translates  $\{\psi(n-qM) = \psi_q(n), \forall q\}$ . In addition, the  $V$  is now considered to be extended over a time interval which is relatively large compared to the N-dimensional t-f space in FIG.

1,2 to avoid end-effects on the analysis. We start by approximating the sequence  $\{z(n), \forall n\}$  by the  $\{\hat{z}(n), \forall n\}$  where:

$$\begin{aligned}\hat{z}(n) &= \sum_q Z_q \psi(n - qM) \\ &= \sum_q Z_q \psi(n_0 + (n_1 - q)M)\end{aligned}$$

where the complex coefficients  $\{Z_q\}$  are derived from the original sequence using the orthogonality properties of  $\psi$

$$\begin{aligned}Z_q &= \sum_n z(n) \psi^*(n - qM) \\ &= \sum_n z(n) \psi_q(n)\end{aligned}$$

5

The following equations prove that the coefficients  $\{Z_q, \forall q\}$  are orthonormal:

$$\begin{aligned}Z_q Z_{q'}^* &= \sum_{\Delta n} z(\Delta n - qM) z^*(\Delta n - q'M) \psi_q(\Delta n) \psi_{q'}^*(\Delta n) \\ &= \delta_{qq'} \sum_n |\psi_q(n)|^2 \quad \text{since the sequence } \{z\} \text{ is orthonormal} \\ &\quad \text{for } qM \text{ time translates} \\ &= \delta_{qq'} \quad \text{with normalization of the energy of } \psi\end{aligned}$$

10

15

Equations (12) and (13) together prove the Karhunen-Loeve's theorem which proves the following equation for the accuracy in approximating the stochastic sequence  $\{z(n), \forall n\}$  by  $\{\hat{z}(n), \forall n\}$ . This accuracy is expressed by the expected "E(o)" squared error "(o)" in this approximation:

$$E\{z(n) - \hat{z}(n)\}^2 = 1 - \sum_{n_1} |\psi(n_0 + n_1 M)|^2 \quad (14)$$

20

We need to prove that the right hand side of this equation is zero which then proves that the approximating sequence is equal to the original sequence in the mean-square sense. In turn this proves that the new waveform coordinates  $\{\psi_q, \forall q\}$  are a basis for the original sequence  $\{z(n), \forall n\}$  which is our goal.

The right hand side of equation (14) when set equal to zero expresses Mercer's theorem so our goal is to prove Mercer's theorem. To do this we use the DFT of  $\psi$  in equation (11) and the coordinates in (10) to evaluate the right hand side of equation (14). We find

$$\begin{aligned}
 1 - \sum_{n_1} |\psi(n + n_1 M)|^2 &= 1 - \sum_{k_0} \sum_{k_0'} \Psi_{k_0} \Psi_{k_0'}^* W_N^{\Delta k_0 n_0} \Gamma \\
 \text{where } \Gamma &= (1/L) \sum_{n_1} W_L^{\Delta k_0 n_1} \\
 &= \sin(\pi \Delta k_0) / L \sin(\pi \Delta k_0 / L) \\
 &= 1 \text{ for } \Delta k_0 = 0 \\
 &= 0 \text{ otherwise}
 \end{aligned} \tag{15}$$

This proves that

$$1 - \sum_{n_1} |\psi(n + n_1 M)|^2 = 0 \quad \forall n_0$$

which proves that equation (14) reduces to

$$E\{z(n) - \hat{z}(n)\}^2 = 0 \tag{16}$$

which as per the above proves that the set of multi-resolution waveforms is a basis. This proof easily generalizes to the multi-resolution waveforms at all of the scales  $\{p\}$  and time

translates  $\{q\}$ , and to the expansion of the harmonic design coordinates over  $2L, 3L, \dots$  as required by the application.

Next we demonstrate that these waveforms have multi-scale properties. The Fourier domain design for the new waveforms provides a natural and easy way to derive the complete set of waveforms  $\{\psi_{p,q}, \forall p,q\}$  for the space  $V$  from the design of the dc waveform  $\psi$  by using the same invariant set of Fourier domain harmonic design coordinates  $\{\Psi_k, \forall k_0\}$  derived for the dc multi-resolution waveform. This demonstration requires that we show 1) how the multi-scale transformations are implemented with the design in the Fourier domain, and 2) how the waveform design remains invariant under scale changes.

First consider the multi-scale transformation which derives the waveforms at the scale and shift parameters "p,q" for the dc waveform at scale "p=0" and centered at the origin "q=0". We begin by extending the parameters and coordinates in equation (10), to include both scaling and subsampling or decimation in a form that is equivalent to the iterated filter bank construction which is used to derive the waveform using the filter scaling functions. Starting with the coordinates at scale "p=0" the parameters and coordinates at scale "p=p" are given by the equations:

p=0 parameters and coordinates

$$n = n_0 + n_1 M \quad (17)$$

$$\begin{aligned} n_0 &= a_0 + a_1 2 + \dots + a_{m-1} 2^{m-1} \\ &= M \text{ points} \end{aligned}$$

$$M = 2^m$$

$$n_1 = b_0 + b_1 2 + \dots + b_{l-1} 2^{l-1}$$

$$= L \text{ points spaced at } M \text{ sample intervals}$$

$$L = 2$$

p=p parameters and coordinates

$$\begin{aligned} 2^{-p} n(\downarrow 2^p) &= \text{scaled by "2}^{-p}\text{"} \\ &\text{and subsampled or decimated by } 2^p:1 \\ &= n_0(p) + n_1(p)M \end{aligned}$$

$$\begin{aligned} 5 \quad 2^{-p} n_0(\downarrow 2^p) &= \text{scaled by "2}^{-p}\text{"} \\ &\text{and subsampled or decimated by } 2^p:1 \\ &= n_0(p) \\ &= a_p + a_{p-1}2 + \dots + a_{p+m-1} 2^{p+m-1} \\ &= M \text{ points spaced at } 2^p \text{ sample intervals} \end{aligned}$$

$$\begin{aligned} 10 \quad 2^{-p} n_1(\downarrow 2^p) &= \text{scaled by "2}^{-p}\text{"} \\ &\text{and subsampled or decimated by } 2^p:1 \\ &= n_1(p) \\ &= b_p + b_{p+1} 2 + \dots + b_{p+1-1} 2^{p+1-1} \\ &= L \text{ points spaced at } M2^p \text{ sample intervals} \end{aligned}$$

15

together with the observation that the sampling interval "T" is increased to "2<sup>p</sup>T" under the scale change from "p=0" to "p=p" and subsampling or decimation from "1:1" to "2<sup>p</sup>:1". Combining these equations with the analytical formulation in (7) and the Fourier domain representation in (11) enables the waveforms at the parameters "p,q" to be written as a function of the Fourier domain harmonic design coordinates:

20

25

$$\begin{aligned} \psi_{p,q,r}(n) &= 2^{-p/2} \psi(2^{-p}n - qM) e^{i2\pi f_c(p,r)nT} \\ &= (2^{-p/2} / N') \sum_{k_0} \Psi_{k_0} W_N^{k_0(n(p)-qM)} e^{i2\pi f_c(p,r)n(p)2^pT} \end{aligned} \quad (18)$$

for all admissible scale, translation, and frequency index parameters "p,q,r".

30

Next we need to demonstrate that the frequency domain design in (11) remains invariant for all parameter changes and in particular for all scale changes. This multi-scale property expresses the accordion behavior of the design in that the Wavelets at different scales are simply the stretched and compressed versions of the mother waveform with the appropriate frequency translation indices. This multi-scale invariancy means that the design for a M=16 channel filter bank remains the same for M=100 or M=10,000 channel filter banks, when the overlap L and the performance goals remain constant. To demonstrate this invariant property across scales, we consider the multi-resolution waveform at scale "p" with the other parameters set equal to zero for convenience "q=0, r=0" and without loss of generality. The Fourier domain frequency response  $\Psi(f)$  can be evaluated starting with the original formulation in equation (7):

DFT at "p, q=0, r=0" (19)

$$\begin{aligned}
 \Psi_p(f) &= (1/N') \sum_{k_0} \Psi_{k_0} \sum_{n(p)} W_{N'}^{-(fN'2^p T - k_0)n(p)} \\
 &= \sum_{k_0} \Psi_{k_0} \left[ \frac{\sin(\pi (fN'2^p T - k_0))}{N' \sin(\pi (fN'2^p T - k_0)/N')} \right] \\
 &= \sum_{k_0} \Psi_{k_0} \text{ [Harmonic interpolation for "k_0"]}
 \end{aligned}$$

This only differs from the harmonic representation in equation (9) in the restriction of the design coordinates to the subset of harmonic coefficients  $\{\Psi_{k_0}, \forall k_0\}$  and the stretching of the time interval to " $2^p T$ " corresponding to the scale " $p=p$ ". The harmonic interpolation functions are observed to remain invariant over scale changes upon observing that the frequency scales as

" $f \sim 1/2^p T$ " which means the "frequency\*time" product remains invariant with scale changes as per the fundamental property of the waveforms. This means the harmonic interpolation functions remain invariant with scale change and therefore the frequency response remains an invariant. This demonstrates the waveform design is an invariant across the waveform scales which means we only need a single design for all scales or resolutions of interest.

LS design algorithms for new waveform will be described to illustrate the advantages our waveform has over current designs. The two LS algorithms described are the eigenvalue and the gradient search which respectively can be reduced to algorithms which are equivalent to current eigenvalue and Remez-exchange waveform design algorithms for application to a uniform filter bank. We consider the t-f space which is spanned by a uniform polyphase filter bank consisting of M channels at the frequency spacing  $f_w = 1/MT$  where T is the digital sampling interval, and the filter waveform FIR time response is stretched over L sampling time intervals  $T_s$ . This polyphase filter bank is ideally decimated which means the filter output sample rate  $1/T_s$  is equal to the channel-to-channel spacing  $T_s = MT$ , equivalent to stating that there is no excess bandwidth  $\alpha = 0$ . Our design for this topology is immediately applicable to an arbitrary set of multi-resolution filters through the scaling equation (18) which gives the design of our waveform at arbitrary scales in terms of our design of the dc waveform.

For this polyphase filter bank used to construct the dc waveform or filter impulse response, our LS example design algorithms will use 5 metrics consisting of the 2 prior art passband and stopband metrics, and the 3 new metrics consisting of the ISI, ACI, and QMF, and solve the LS minimization problem using as design coordinates the subset of harmonic coordinates

which are a basis. Since our two example LS design algorithms only differ in the use of an eigenvalue LS optimization and the use of a gradient search LS optimization, the flow diagrams for the construction of the cost functions and the solution for the optimal waveform will be identical. However, there are differences in the construction of the cost functions from the respective metrics and in the iterative solution mathematics. Both LS solutions for the harmonic design coordinates minimize the weighted sum of the error residuals or cost functions from the 5 metrics. These design coordinates for are the Fourier harmonics  $\{\psi_{k_0}, \forall k_0\}$  for  $\{k_0 = 0, 1, \dots, L-1\}$ . Resulting algorithms are easily extended to the applications requiring the design coordinates to cover  $2L, 3L, \dots$  harmonics.

Frequency domain design coordinates are related to the waveform time domain digital samples or coordinates as follows.

Mappings of frequency to time (20)

Time domain design coordinates  $\{\psi(n), \forall n\}$  are real and symmetric and can be represented by the reduced set  $\{h_t(n), n=0, 1, \dots, ML/2\}$

$$\begin{aligned} h_t(n) &= \psi(0) \quad \text{for } n=0 \\ &= 2\psi(n) \quad \text{for } n=1, 2, \dots, ML/2 \\ &= \text{time domain design coordinates} \end{aligned}$$

Frequency domain harmonic design coordinates  $\{\psi_{k_0}, \forall k_0\}$  are real and symmetric and can be represented by the reduced set  $\{h_f(k), k=0, 1, \dots, L-1\}$

$$\begin{aligned} h_f(k) &= \psi_{k_0} \quad \text{for } k=k_0=0 \\ &= 2\psi_{k_0} \quad \text{for } k=k_0=1, 2, \dots, L-1 \\ &= \text{frequency domain design coordinates} \end{aligned}$$



Mapping of the frequency coordinates  $\{h_f(k), k=0,1,\dots,L-1\}$  into the time coordinates  $\{h_t(n), n=0,1,\dots,ML/2\}$  is defined by the matrix transformation

$$h_t = B h_f$$

where

$$h_f = (h_f(0), \dots, h_f(ML/2))^t \text{ transpose of column vector}$$

$$h_t = (h_t(0), \dots, h_t(ML/2))^t \text{ transpose of column vector}$$

$$B = (ML/2 + 1) \times L \text{ matrix}$$

$$= [ B_{kn} ] \text{ matrix of row } k \text{ and column } n \text{ elements } B_{kn}$$

$$B_{kn} = 1 / ML \text{ for } n=1$$

$$= 2 \cos(2\pi kn / ML) \text{ otherwise}$$

wherein the  $N'=ML+1$  has been replaced by  $ML$  since a single end point has been added to the the FIR to make it symmetrical for ease of implementation for the example Wavelet being considered with a sample at the mid-point that makes the number of samples  $N'$  an odd number.

20

Passband and stopband metrics and cost functions are derived with the aid of FIG. 3 which defines the power spectral density (PSD) parameters of interest for the passband and stopband of the PSD  $\Psi(\omega)$  for communications applications.

25 Requirements for radar applications include these listed for communications. Referring to FIG. 3 the passband 11 of the waveform PSD is centered at dc ( $f=0$ ) since we are designing the dc or baseband waveform, and extends over the frequency range  $\omega_p$  extending from  $-\omega_p/2$  to  $+\omega_p/2$  12 in units of the radian

30 frequency variable  $\omega=2\pi fT$  13 where  $T$  is the digital sampling interval defined in FIG. 1. The frequency space extends over the range of  $f=-1/2T$  to  $f=+1/2T$  which is the frequency range in FIG 1 translated by  $-1/2T$  so that the dc waveform is at the center of the frequency band. Quality of the PSD over the

passband is expressed by the passband ripple 14. Stopband 15 starts at the edge 16 of the passbands of the adjacent channels  $\pm\omega_a/2$  16 and extends to the edge of the frequency band  $\omega=\pm\pi$  17 respectively. Stopband attenuation 18 at  $\pm\omega_a/2$  measures the PSD isolation between the edge of the passband for the dc waveform and the start of the passband for the adjacent channels centered at  $\pm\omega_s$  19. Rolloff 20 of the stopband is required to mitigate the spillover of the channels other than the adjacent channels, onto the dc channel. Deadband or transition band 21 is the interval between the passbands of contiguous channels, and is illustrated in FIG. 3 by the interval from  $\omega_p/2$  to  $\omega_a/2$  between the dc channel and adjacent channel at  $\omega_a$ . Waveform sample rate  $\omega_s$  22 is the waveform repetition rate. For the LS example algorithms, the waveform sample rate is equal to the channel-to-channel spacing for zero excess bandwidth. Therefore,  $1/T_s = \omega_s/2\pi T = 1/MT$  which can be solved to give  $\omega_s = 2\pi/M$  for the radian frequency sampling rate of the filter bank which is identical to the waveform repetition rate.

We start by rewriting the DFT equations for the dc waveform in (11) as a function of the  $\{h_f(k), k=0,1,\dots,L-1\}$

$$\begin{aligned}\psi(\omega) &= \sum_n \psi(n) \cos(n\omega) \\ &= c^t B h_f \quad \text{using (21) and the definition of the vector "c"} \\ c &= (1, \cos(\omega), \dots, \cos((ML/2)\omega))^t \text{ transpose of column vector}\end{aligned} \tag{21}$$

which is equivalent to the equation for  $\psi(\omega)$  in (9) expressed as a linear function of the  $\{h_f(k), k=0,1,\dots,L-1\}$ . An ideal "c" vector "c<sub>r</sub>" will be introduced for the passband and the stopband in FIG. 3 in order to identify the error residual  $\delta\psi(\omega)$  at the frequency " $\omega$ " in meeting the ideal passband and stopband

requirements. The ideal PSD is flat and equal to "1" for the passband, and equal to "0" for the stopband. We find

5 Error residuals for passband and stopband (22)

$$\begin{aligned} c_r &= (1, 1, \dots, 1)^t \quad \text{passband ideal "c"} \\ &= (0, 0, \dots, 0)^t \quad \text{stopband ideal "c"} \end{aligned}$$

$$\delta c = c_r - c \quad \text{error vector}$$

10 
$$\delta \psi(\omega) = \delta c^t B h_f$$
  

$$= \text{Residual error in meeting the ideal spectrum at "}\omega\text{"}$$

The LS metric for the passband and stopband can now be constructed as follows for the eigenvalue and the LS optimization  
 15 (or equivalently, the LS algorithm) design algorithms

Passband and stopband metrics (23)

20 
$$J(\text{band}) = \frac{1}{\text{band}} \int_{\text{band}} |\delta \psi(\omega)|^2 d\omega \quad \text{Eigenvalue}$$
  

$$= h_f^t R h_f \quad \text{Eigenvalue}$$
  

$$= \|\delta \psi\| \quad \text{LS}$$

25 where

$$\begin{aligned} \text{band} &= [0, \omega_p) \quad \text{passband} \\ &= (\omega_s, \pi] \quad \text{stopband} \\ R &= \frac{1}{\text{band}} \int_{\text{band}} (B^t \delta c \delta c^t B) d\omega \\ &= L \times L \text{ matrix} \end{aligned}$$

$\delta\psi = ( \delta\psi(\omega_1) , \dots , \delta\psi(\omega_u) )^t$   
 = vector of error residuals at the  
 frequencies  $\omega_1 , \dots , \omega_u$  across the band  
 $\|(\mathbf{o})\|$  = norm or length of the vector (o) and which  
 includes a cost function for the errors of  
 the individual components.

5

where it is observed that the eigenvalue approach requires that  
 the LS metrics be given as quadratic forms in the design  
 coordinates  $\{h_f(k), k=0,1,\dots,L-1\}$  whereas with the LS approach it  
 is sufficient to give the LS metrics as vector norms with  
 imbedded cost functions or an equivalent formulation.

QMF metrics express the requirements on the deadband that  
 the PSD's from the contiguous channels in FIG. 3 add to unity  
 across the deadband  $[\omega_p, \omega_s]$  in order that the filters be QMF  
 filters. By suitable modification of the error vector  $\delta c$ , the  
 previous construction of the passband and stopband metrics can be  
 modified to apply to the deadband. We find

Deadband metrics (24)

$$\begin{aligned}
 J(\text{deadband}) &= \frac{1}{\text{deadband}} \int_{\text{deadband}} \|\delta\psi(\omega)\|^2 d\omega && \text{Eigenvalue} \\
 &= h_f' R h_f && \text{Eigenvalue} \\
 &= \|\delta\psi\| && \text{LS}
 \end{aligned}$$

(24) continued

where

$$\delta c = c_r - c(\omega) - c(\pi/M - \omega)$$

30

where  $c(\omega)=c$  as defined in (22) and (23), and  $c(\pi/M - \omega) = c$  at the offset frequency " $\pi/M - \omega$ " corresponding to the overlap of the contiguous filters over the deadband.

5

Orthonormality metrics measure how close we are able to designing the set of waveforms to be orthonormal over the t-f space, with the closeness given by the ISI and the ACI. ISI and ACI errors are fundamentally caused by different mechanisms and therefore have separate metrics and weights to specify their relative importance to the overall sum of the LS metrics. ISI is a measure of the non-orthogonality between the stream of waveforms within a channel as per the construction in FIG. 3. On the other hand, ACI is a measure of the non-orthogonality between the waveform within a channel and the other waveforms in adjacent channels. This means the stopband performance metric has a significant impact on the ACI due to the sharp rolloff in frequency of the adjacent channel, and the ACI metric is then a measure of the residual non-orthogonality due to the inability of the stopband rolloff in frequency from completely eliminating the ACI errors.

We assume that the received waveform is identical to the filter waveforms and is transmitted at the filter output sample intervals equal to  $MT$  seconds. The second assumption means we are assuming the receiver is synchronized with the received signal. Since there is no information lost by sampling asynchronously with the received waveform, we are free to make this synchronization assumption without loss of generality. ISI metrics are derived in the following set of equations.

Mapping of  $h_f$  into  $\psi$

$\psi = (\psi(-ML/2), \dots, \psi(ML/2))^t$  transpose of column vector

5

$= H h_f$

$H = (ML+1) \times L$  matrix of elements  $H_{kn}$

$H_{kn} = 1$  for  $n=1$

$= 0.5 \cos(2\pi kn/ML+1)$  otherwise

Offset matrix  $A$

10

$A = L \times (ML+1)$  matrix of elements  $A_{kn}$

$A_{kn} = 0$  for  $k=1$

$= [0 \quad 0 \quad \dots \quad \psi(-ML/2) \quad \dots \quad \psi((L-k)M+1)]$  (25) continued  
           1   2                    kM                   LM+1

15

ISI error vector  $\delta E$

$\delta E = L \times 1$  column vector

$= A H h_f$

20

ISI metric

$J(\text{ISI}) = \delta E^t \delta E$  Eigenvalue

$=$  Non-linear quadratic function of  $h_f$

$= \|\delta E\|$  LS

25 ACI metrics are derived using the ISI metric equations with the following modifications.

ACI metrics

(26)

30

Mapping of  $h_f$  into  $\psi$  is the same as developed for ISI

Offset matrix  $A$  elements are changed as follows to apply to Channel 1:

$A_{kn} = 0$  for  $k=1$

$$= [0 \quad 0 \quad \dots \quad \psi(-ML/2) W_M^0 \quad \dots \quad \psi((L-k)M+1) W_M^{(L-k)}]$$

1      2                      kM+1                                  LM+1

which means the ACI error vector  $\delta E$  is

$$\begin{aligned} \delta E &= L \times 1 \text{ column vector} \\ &= A H h_f \end{aligned}$$

ACI metric for the two contiguous channels

$$\begin{aligned} J(\text{ISI}) &= 2 \delta E^t \delta E && \text{Eigenvalue} \\ &= \text{Non-linear quadratic function of } h_f \\ &= 2 \|\delta E\| && \text{LS} \end{aligned}$$

where the factor "2" takes into account there are two contiguous channels or one on either side of the reference channel 0 in FIG. 3. Because of the fast rolloff of the frequency spectrum the addition of more channels into the ACI metric is not considered necessary, although the functional form of the ACI metric in (26) allows an obvious extension to any number of adjacent channels which could contribute to the ACI.

Cost function J for the LS algorithms is the weighted sum of the LS metrics derived in (23), (24), (25), (26). The LS algorithms minimize J by selecting the optimal set of frequency coordinates  $\{h_f(k), \forall k\}$  for the selected set of parameters used to specify the characteristics of the dc waveform, frequency design coordinates, LS metrics, and weights. Cost function and optimization techniques are given by the equations

Cost function J (27)

$$\begin{aligned} J &= \sum_x w(\text{metrics}) J(\text{metrics}) \\ &= \text{weighted sum of the LS metrics } J(\text{metrics}) \end{aligned}$$

where

metrics = passband, stopband, deadband, ISI, ACI

$\{w(metrics), \forall metrics\}$  = set of weights

$$\sum_x w(metrics) = 1 \quad \text{normalization}$$

5 Optimization goal

Goal: minimize  $J$  with respect to the selection of  
the  $\{h_f(k), \forall k\}$

10 Optimization algorithms

Two algorithms are the Eigenvalue and the LS optimization  
where the eigenvalue optimization algorithm uses the non-  
linear quadratic formulations of the LS metrics and the LS  
optimization algorithm uses the norm formulations for the  
15 LS metrics.

FIG. 4 is a summary of the LS metrics and the construction  
of the cost function  $J$ . Design parameters **23** are the input and  
20 output design parameters. Input parameters are the number of  
polyphase channels  $M$  or equivalently the number of digital  
samples at spacing  $T$  over the symbol interval  $T_s = MT$ , the length  
of the FIR time response for the waveform in units of  $L$  which are  
the number of digital samples per waveform repetition interval  $T_s$   
25 so that the total number of digital samples for the symmetric FIR  
time response is equal to  $ML+1$ , number of DFT samples per FIR  
length  $n_{fft}$  for implementation of the LS algorithms, passband  
radian frequency  $\omega_p$ , stopband radian frequency  $\omega_s$ , waveform  
repetition rate in radian frequency  $\omega_s$ , selection of the set of  
30 design coordinates  $\{h_f\}$  to be used in the optimization, and the  
metric weights  $\{w(metrics)\}$ . Output parameters are the set of  
harmonic design coordinates  $\{h_f\}$  that minimize  $J$ . Band metrics  
**24** are the passband, stopband, and deadband metrics defined in



equations (23), (23), (24) respectively. Interference metrics  
25 are the ISI and ACI metrics defined in equations (25) and  
(26) respectively. LS cost function J 26 is the weighted  
linear sum of the metrics defined for the band 24 and the  
5 interference 25 as defined in equation (27).

FIG. 5A,5B,. . . ,5P,5Q are the Matlab 5.0 code for the LS  
recursive eigenvalue solution algorithm used to design the  
Wavelet Wavelet in FIG.6. Included are a listing of the frequency  
10 domain design harmonics, time response, and data plotting  
software used in the optimization, and an example of the scaling  
of this mother Wavelet into a Wavelet with new scaling  
(dilation), time translation, frequency translation parameters,  
and the functions used in the code. The Matlab code uses an  
15 iterative approach to find the optimal frequency domain  
eigenvector solution to the quadratic form for the LS error whose  
error matrix is the weighed sum of the error matrices for the  
stopband, passband, deadband metrics and the error matrices for  
the ISI and ACI metrics which are functions of the eigenvectors.  
20 For each iteration the ISI and ACI error matrices are constructed  
with the frequency domain eigenvectors from the previous  
iteration. The iteration finds the new frequency domain  
eigenvectors which are then used to update the ISI and ACI  
metrics for the next iteration. This iteration is repeated until  
25 there is convergence. The Matlab code allows the operator to  
update the metric weights as well as the scenario parameters to  
find the optimal choice for the performance goals.

FIG 5A Matlab code starts with the selection of the design  
30 parameters in 29 Step 1. Step 1.1 lists the scenario parameters  
which are M=16 digital samples per Wavelet  $\psi$  sample interval,  
L=16 nominal length of Wavelet  $\psi$  in units of M, N=ML+1 Wavelet  $\psi$   
length which is represented by N' in equations (10), fs=1 is the  
normalized channel spacing equal to the Wavelet  $\psi$  sample rate,

$fp=0.8864$  is the passband frequency interval,  $n_f=16$  is the number of design frequency harmonics,  $n\_fft=1024$  is the number of digital samples used for calculation of the frequency spectrum centered at 0 frequency.  $ebno=E_b/N_0=6.0$  dB is the design value of the energy per bit  $E_b$  to noise power density  $N_0$  ratio, and  $x\_imbal\_aci=6.0$  dB is the assumed channel-to-channel power imbalance used in the calculation of the ACI errors. Step 1.2 derives the software parameters from the design parameters in Step 1.1. Step 1.3 lists the optimization parameters which are the number of iterations  $n\_iteration = 10$ , and the metric weights  $w(metric)$  from equation (27) and in FIG. 4 equal to  $w(pass)=\alpha_1=1.e-2$  for passband,  $w(stop)=\alpha_2=0.80$  for stopband,  $w(ISI)=\alpha_3=2.e-3$  for ISI,  $w(ACI)=\alpha_4=0.5$  for ACI, and  $w(dead)=\alpha_5=0$  for deadband. The number of iterations was selected to provide a convergent solution for the weighted LS error metrics  $w(metric)J(metric)$  in FIG. 5K 38 Step 10 figure(2) in the Matlab code and for their sum  $J$  in figure(1) in the Matlab code. Weight values were selected to optimize the Wavelet  $\psi$  filter performance in FIG. 6 and in figure(3) in the Matlab code in FIG. 5L 39 Step 11, Wavelet  $\psi$  ripple, ISI, ACI signal-to-noise SNR power ratio losses in figure(4) in the Matlab code, and Wavelet  $\psi$  time response in figure(5) in the Matlab code.

FIG. 5B 30 Step 2 are the initialization calculations prior to the start of the iteration loop. Step 2.1 calculates the one-sided Wavelet  $\psi$  length parameter  $m=128$ . Step 2.2 calculates the matrix transformation  $bw\_matrix$  which maps the  $\psi$  frequency domain design eigenvectors into the one-sided  $\psi$  time response. Step 2.3 refers to the function  $pmn$  in FIG. 5P, 5Q 41 in Step 13.1 which computes the LS error matrix which is the sampled data integral  $\Sigma[\delta c \delta c'] d\omega$  over the band in equation (23) for the the passband and stopband metrics  $J(pass), J(stop)$ . The function  $pmn\_d$  computes the corresponding integral over the deadband in equation (24) and is not listed since it was not used for FIG. 6. Step

2.4 constructs a structural matrix  $c\_matrix$  used in the ISI and ACI calculations. Step 2.5 constructs the sample rate templates for the passband upper edge, sample rate marker, and passband lower edge for frequency performance evaluation.

5

FIG. 5C 31 Step 3 uses the function  $p_{mn}$  to compute the LS error matrices passband and stopband in Steps 3.1, 3.2. Deadband LS error matrix deadband is set equal to a null matrix in Step 3.3. Step 3.4 computes the matrix  $p\_total$  equal to the weighted sum of these matrices. Step 3.5 maps this LS error matrix  $p\_total$  in the time domain into the LS error matrix  $pw\_t$  in the frequency domain using the matrix transformation  $bw\_matrix$ .

FIG. 5C,5D 32 Step 4 initializes matrices used in the iteration loop and starts the iteration loop for the iterations  $i\_iteration=1,...,10$ . Step 4.1 calculates the eigenvalue and eigenvector which minimize the cost function  $J$  in equations (27) and FIG. 4 whose LS error matrix is  $pw\_t$ . Step 4.2 uses the  $bw\_matrix$  to map the eigenvector in frequency into the Wavelet time response  $\psi=hn$  and stores the eigenvector as the set of Wavelet  $\psi$  design harmonics  $\psi_k=hw\_eig(k)$  for  $k=0,1,...,15$  where  $\psi_k$  has been defined in equations (9) and in equations (11) upon recognizing that there are  $n\_f=16=L$  design harmonics  $k_0=k=0,1,...,15$ . There is no reason to use the negative harmonics since the spectrum is real and symmetric about the 0 frequency. Step 4.3 computes the passband peak-to-peak ripple as  $xripple$  and the stopband attenuation as  $xstop$ .

FIG. 5E 33 Step 5 calculates the weighted passband error metric  $w(pass)J(pass)=beta\_pass$ , weighted stopband error metric  $w(stop)J(stop)=beta\_stop$ , and weighted deadband error metric  $w(dead)J(dead)=beta\_dead$  in equations (27) using the  $b\_vector$  format for  $hn$  and the LS error matrices passband, stopband, deadband.

FIG. 5E,5F 34 Step 6 calculates the ISI and ACI LS error matrices, their metrics, and their error contributions to the SNR loss. Step 6.1 calculates the ISI LS error matrix  $w\_matrix$  and the corresponding ISI metric  $J(ISI)=errM\_isi$  with Matlab code which implements equations (25), and calculates the ISI residual error  $errV\_isi$  that causes an ISI SNR loss. Step 6.2 calculates the ACI LS error matrix  $w\_f\_matrix$  and the corresponding ACI metric  $J(ACI)=errM\_aci$  with Matlab code which implements equations (26), and calculates the ACI residual error  $errV\_aci$  that causes a ACI SNR loss.

FIG. 5G 35 Step 7 calculates the weighted LS error metrics for ISI and ACI and the LS error matrix  $pw\_t$  for the next iteration. Step 7.1 calculates the weighted ISI LS error metric  $w(ISI)J(ISI)=beta\_isi$  and the weighed ACI LS error metric  $w(ACI)J(ACI)=beta\_aci$  in equations (27) and the sum of the weighted LS error metrics  $J=errM\_isi$ . Step 7.2 saves the weighted LS error metrics and their sum  $J$  for each iteration. Step 7.3 updates the  $pw\_t$  matrix for the next iteration.

FIG. 5G,5H 36 Step 8 calculates the SNR losses, stores these losses for each iteration, and completes the iteration loop. Step 8.1 computes the SNR loss in dB due to passband ripple as  $xloss\_ripple$ , due to ISI as  $xloss\_isi$ , due to ACI as  $xloss\_aci$ , and the total SNR loss as  $xloss\_total$ . Step 8.2 saves these SNR losses for each iteration and completes the iteration loop.

FIG. 5H,5I,5J,5K 37 Step 9 documents the Wavelet  $\psi$  frequency design harmonics and time response generated by the Matlab code for the Wavelet in FIG. 6. Step 9.1 lists the Wavelet  $\psi$  frequency domain harmonic design coordinates  $\psi_k(k)=hw\_eig(k)$  for harmonics  $k=0,1,...,15$ . Only the positive

harmonics are listed since the frequency spectrum is real and symmetric about  $k=0$ . Step 9.2 lists the Wavelet  $\psi$  time response  $\psi(n)=hn(n)$  for  $n=0,1,2,\dots,128$  with the coordinate frame centered at the Wavelet peak. Only the positive digital samples  
5 are listed since the time response is real and symmetric about  $n=0$ .

FIG. 5K 38 Step 10 plots the total weighted LS error metric  $J$  in figure(1) and the individual weighted LS error metrics in  
10 figure(2) as functions of the iteration number. After about 6-7 iterations both the total and the individual weighted LS error metrics are observed to stabilize indicating that the selected number of iterations  $n\_iteration=10$  is sufficient for convergence.

15 FIG. 5L 39 Step 11 plots the Wavelet  $\psi$  frequency response in figure(3) in the Matlab code which is the same as the frequency response in FIG. 6, plots the SNR losses due to passband ripple, ISI, ACI and the total loss in figure(4) in the  
20 Matlab code, and plots the time response in figure(5) in the Matlab code for use in the optimization of the LS metric weights in Step 1.3 as well as the scenario parameters in Step 1.1.

FIG. 5M 40 Step 12 documents the Matlab code to rescale the  
25 mother Wavelet  $\psi$  in FIG. 6 which was derived in the previous Matlab code in Steps 1-11, for new scale (dilation)  $p$ , time translation  $q$ , and frequency translation  $k$  parameters compared to the values  $p=0, q=0, k=0$  for the mother Wavelet  $\psi$ . An example set of new parameters documented in the code is  $p=2, q=2, k=3$  and  
30 with the assumption that the digital sampling rate remains fixed under the parameter change. A constant digital sample rate keeps the frequency band constant under the parameter change.

FIG. 5M 40 Step 12.1 defines the new Wavelet  $\psi_{p,q,k}$  in equations (7), (18) resulting from these parameter changes, in equations (28)

5 New Wavelet scaled from mother Wavelet (28)

$$\psi_{p,q,k} = 2^{-p/2} \psi(2^{-p}n - qM) \exp(j2\pi k 2^{-p}n / ML)$$

10 Case 1 Scaled (dilated) sampling  $2^{-p}n$  with fixed M  
subsamples (decimates) n by the factor  $2^p$

• Represent n as

$$n = n_0 + 2^p n_p$$

$$n_0 = 0, 1, \dots, 2^p - 1$$

$$n_p = 0, +/ -1, +/ -2, \dots$$

15 • We observe  $2^{-p}n = n_p$

• This enables the new Wavelet to be written

$$\psi_{p,q,k} = 2^{-p/2} \psi(n_p - qM) \exp(j2\pi k n_p / ML)$$

20 Case 2 Sampling n remains fixed and M is  
rescaled by the factor  $2^p$

• New M is  $M_{\text{new}}$

$$M_{\text{new}} = 2^p M$$

• This enables the new Wavelet to be written

$$\psi_{p,q,k} = 2^{-p/2} \psi(n - qM_{\text{new}}) \exp(j2\pi kn / M_{\text{new}}L)$$

25

wherein the new Wavelet equation from (7), (18) is re-written using the frequency translation parameter  $k=r$  and the explicit frequency translation expression  $\exp(j2\pi k 2^{-p}n / ML)$  which is  
30 recognized as the discrete Fourier transform kernel.

In Case 1 in equations (28) corresponding to the standard Wavelet assumption, the subsampling or decimation of n by the factor  $2^p$  stretches the time between contiguous samples by the

factor  $2^p$  while keeping constant the number of samples  $M$  per Wavelet  $\psi$  sample interval, and therefore reduces the frequency band by the factor  $2^p$ . The new  $n$  can be represented as the sum of the two fields  $n_0 = 0, 1, \dots, (2^p - 1)$  and  $n_p = 0, +/-1, +/-2, \dots$ . Scaling or equivalently subsampling results in the new  $n$  equal to  $n_{\text{new}} = 2^{-p} n = n_p$  corresponding to a stretching of the sample interval by  $2^p$ . The new Wavelet length  $N_{\text{new}}$  remains constant  $N_{\text{new}}=N$  using the  $n_p$  sampling.

10 In Case 2 in equations (28) which is the communications application being considered, the sampling is held constant corresponding to a constant frequency band assumption. The factor  $2^{-p}$  is divided out in the Wavelet expression which is equivalent to the  $M$  being scaled to  $M_{\text{new}}=2^p M$  corresponding to increasing  
15 the number of samples per Wavelet interval by the factor  $2^p$ . This means Case 2 corresponds to increasing the maximum number of channels by the factor  $2^p$  over the same frequency band. The new Wavelet length is equal to  $N_{\text{new}}=M_{\text{new}}L+1 = 1025$  since  $M_{\text{new}}=2^p M=64$ .

20

FIG. 5M 40 Step 12.2 derives the new matrix transformation  $bw\_matrix\_new$  which maps the  $\psi$  frequency domain design eigenvectors into the one-sided  $\psi$  time response.

25 FIG. 5M, 5N 40 Step 12.3 uses the matrix transformation  $bw\_matrix\_new$  to map the design eigenvector  $hw\_eig$  into the new Wavelet in three steps. In the first step, the mother Wavelet is translated into the new baseband Wavelet  $\psi_{p,q=0,k=0} = hn_0$  which is the mother Wavelet scaled by  $p$  and with no time and frequency  
30 translations  $q=k=0$ . The second step translate this baseband Wavelet by  $qM_{\text{new}}$  to generate  $\psi_{p,q,k=0} = hn_1$ . The last step translates this Wavelet  $\psi_{p,q,k=0} = hn_1$  in frequency to give the new Wavelet  $\psi_{p,q,k} = hn_{\text{new}}$ .

FIG. 5N 40 Step 12.4 plots the Wavelet time responses for the mother Wavelet  $\psi=hn$  and the new Wavelet  $\psi_{p,q,k} = hn\_new$  in figure(6) in the Matlab code. FIG. 50 Step 12.5 plots the Wavelet frequency responses for the mother Wavelet  $\psi=hn$  and the new Wavelet  $\psi_{p,q,k} = hn\_new$  in figure(7) in the Matlab code versus the normalized frequency/ $(\psi=hn$  sample rate) and in figure (8) in the Matlab code versus the normalized frequency/ $(\psi_{p,q,k} = hn\_new$  sample rate).

FIG. 5P 41 Step 13 documents the functions used in the Matlab code. Step 13.1 is the code for the function pmn which computes the matrix for the J(BAND) in equations (23). FIG. 5Q 41 Step 13.2 lists the code for the function freq\_rsp which computes the Fourier transform of the input hn versus the normalized frequency/ $(\text{Wavelet } \psi=hn \text{ sample rate})$ .

Applications of this new invention to both communications and radar will be given using these example algorithms and other algorithms supported by this invention. These new waveforms are considered for the applications: 1) to replace the square-root raised cosine waveform (sq-root rc) which is extensively used for the third generation (3G) CDMA communications, 2) to replace the Gaussian minimum shift keying (GMSK) waveform for constant amplitude bandwidth efficient (BEM) applications, and 3) as a candidate waveform for synthetic aperture radar (SAR) and real aperture radar (RAR) applications.

CDMA communications application for the current and the new 3G CDMA considers a waveform designed with this new invention as a possible replacement for the sq-rt rc waveform with bandwidth expansion parameter  $\alpha=0.22$  to  $\alpha=0.40$ . This notation means that for  $\alpha=0.22$  the spectral efficiency is  $(\text{symbol rate}/\text{bandwidth}) = 1/1+\alpha = 1/1.22 = 0.82 = 82\%$ . A basic advantage of the waveform is the potential for a symbol rate increase within the same



bandwidth with an increase in the spectral efficiency to  $\approx 100\%$  depending on the application and operational constraints. The dc power spectral density or power spectrum (PSD) of the waveform is compared to the PSD for the sq-rt r-c in FIG. 6. Plotted are the measured PSD in dB **42** versus the frequency offset from dc expressed in units of the symbol rate **43**. Plotted against the normalized frequency offset are the dc PSD for the new waveform **44**, the sq-rt r-c with  $\alpha=0.22$  **45**, and the sq-rt r-c with  $\alpha=0.40$  **46**. It is observed that the PSD for the new waveform rolls off faster than that for the sq-rt r-c which means that the new mr waveform will support an increased symbol rate for a given available frequency band while satisfying the inherent requirements for low ISI and MAI (multiple access interference).

Constant amplitude BEM application of the new waveform indicates that it is a viable candidate for replacing the current preferred modulation waveform which is the GMSK. The GMSK finds applications for transmitters which operate their HPA(s) amplifiers in a saturation mode in order to maximize their radiated power from the HPA(s), and which require a BEM PSD to avoid excessive spreading of the transmitted power. Simulation data for the dc PSD is plotted in FIG. 7 for the new waveform BEM and the GMSK. Plotted are the measured dc PSD in dB **47** versus the frequency offset from dc expressed in units of the bit rate **48**. Plotted against the normalized frequency offset are the dc PSD for the new waveform BEM **49** and the GMSK **50**, for a length parameter  $L=10$  where  $L$  is the length of the phase pulse in terms of the phase pulse repetition rate. The significance of this example data is that the new waveform has the potential to be designed to offer a PSD which is less spread out than the current GMSK, and therefore an improved BEM waveform.

Radar RAR and SAR application of the waveform indicates that it is a viable candidate to replace the current chirp

waveforms for wideband signal transmission, when combined with pseudo-random phase codes. Results of the simulation for the new waveform and an unweighted frequency chirp waveform are given in FIG. 8. Plotted are the ambiguity function for the new waveform 51 and the unweighted frequency chirp waveform 52. The dc 2-dimensional radar ambiguity function 53 is plotted as a function of the frequency offset in units of  $fT_p$  and the time offset in units of  $t/T_c$  where  $T_p$  is the phase-coded radar pulse length or length of the phase code and  $T_c$  is the phase code chip length. The chip length is identical to the waveform repetition interval  $T_s$  so that  $T_c = T_s$ . It is observed that the new waveform has the potential for significant improvements in the ambiguity function and by implication in the performance.

Preferred embodiments in the previous description are provided to enable any person skilled in the art to make or use the present invention. The various modifications to these embodiments will be readily apparent to those skilled in the art, and the generic principles defined herein may be applied to other embodiments without the use of the inventive faculty. Thus, the present invention is not intended to be limited to the embodiments shown herein and is to be accorded the wider scope consistent with the principles and novel features disclosed herein.